The Astrophysical Journal, 997:143 (16pp), 2026 February 1 https://doi.org/10.3847/1538-4357/ae2798

Galaxy and Mass Assembly (GAMA). The Properties of Quasar Host Galaxies: Star Formation Histories and Stellar Populations

Maria B. Stone[1,2,3], Roberto De Propris[2,4], Clare Wethers[5], Jari Kotilainen[1,2], Nischal Acharya[6], Benne Holwerda[7], Andrew M. Hopkins[8], and Kevin Pimbblet[9,10]
[1] Department of Physics and Astronomy, University of Turku, Vesilinnantie 5, FI-20014, Turku, Finland; mbstone12@gmail.com
[2] Finnish Centre for Astronomy with ESO (FINCA), University of Turku, Vesilinnantie 5, FI-20014, Turku, Finland
[3] Institute for Space Astrophysics and Planetology (IAPS), National Institute for Astrophysics (INAF), via del Fosso del Cavaliere 100, 00133, Rome, Italy
[4] Department of Physics and Astronomy, Botswana International University of Science and Technology (BIUST), Private Bag 16, Palapye, Botswana
[5] Department of Space, Earth and Environment, Chalmers University of Technology, Onsala Space Observatory, 439 92, Onsala, Sweden
[6] Donostia International Physics Center (DIPC), Paseo Manuel de Lordizabal 4, E-20018 Donostia-San Sebastian, Spain
[7] Department of Physics and Astronomy, University of Louisville, 102 Natural Sciences Building, Louisville, KY 40292, USA
[8] School of Mathematical and Physical Sciences, 12 Wally's Walk, Macquarie University, NSW 2109, Australia
[9] E.A. Milne Centre, Faculty of Science and Engineering, University of Hull, Cottingham Road, Kingston-upon-Hull HU6 7RX, UK
[10] Centre of Excellence for Data Science, AI, and Modelling (DAIM), University of Hull, Cottingham Road, Kingston-upon-Hull, HU6 7RX, UK
Received 2024 April 30; revised 2025 November 5; accepted 2025 November 26; published 2026 January 20

Abstract

We investigated the star formation history and stellar populations of a sample of 205 Type I quasar host galaxies ($0.1 < z < 0.35$) and compared them with normal (nonactive) galaxies of the same mass and redshift within the volume of the Galaxy and Mass Assembly redshift survey. We find that quasar host galaxies tend to be star-forming galaxies (∼80%) lying on the star-forming main sequence; the fraction of quasar host galaxies that are quiescent (∼20%) is lower than the fraction of quiescent galaxies in the comparison sample of normal galaxies (54%). We find that the mean star formation rate (SFR) of quasar host galaxies has increased over the past 100 Myr by a factor of 2–3, but these galaxies were star-forming at all times previously. Our data are more consistent with quasar activity originating together with an increase in the SFR of otherwise normal galaxies, similar to episodic star formation in normal spirals. We argue that this indicates that secular processes and minor mergers may be the favored triggers of nuclear activity in the local Universe.

Unified Astronomy Thesaurus concepts: Galactic and extragalactic astronomy (563); AGN host galaxies (2017); Galaxies (573); Quasars (1319); Extragalactic astronomy (506); Star formation (1569); Spectral energy distribution (2129); Supermassive black holes (1663)

1. Introduction

All massive galaxies contain supermassive black holes (SMBHs) in their nuclei (e.g., J. Magorrian et al. 1998; J. Silk & M. J. Rees 1998; K. Gebhardt et al. 2000). The mass of these black holes correlates tightly with the mass (or velocity dispersion) of their parent spheroids (e.g., K. Gültekin et al. 2009), despite very large (several orders of magnitude) differences in the size and mass of these two components. This points to a mechanism of coevolution between SMBHs and their parent galaxies (see J. Kormendy & L. C. Ho 2013 for a review, however see K. Jahnke & A. V. Macciò 2011 for a critique) such as "quasar-mode" feedback (e.g., B. A. Terrazas et al. 2020), where accretion of matter into an SMBH, leads to the triggering of an active galactic nucleus (AGN), and can inject enough energy into the galaxy to affect its star formation through heating, ionization by the ultraviolet flux, or mechanical input from jets (e.g., G. L. Granato et al. 2004; A. C. Fabian 2012; K. Zubovas et al. 2013; A. King & K. Pounds 2015; K. Zubovas & M. A. Bourne 2017; R. Blandford et al. 2019; J. Trussler et al. 2020). However, these outflows and jets can also boost star formation (e.g., P. F. Hopkins 2012; S. Nayakshin & K. Zubovas 2012; K. Zubovas et al. 2013; R. Bieri et al. 2016; K. Zubovas & M. A. Bourne 2017), and even form stars inside the outflow (e.g., W. Ishibashi & A. C. Fabian 2012; K. Zubovas et al. 2013; K. El-Badry et al. 2016; X. Wang & A. Loeb 2018). These mechanisms may also coexist within the same object (e.g., G. Cresci et al. 2015; J. Shin et al. 2019; A. Mandal et al. 2021).

Previous studies (e.g., N. V. Asari et al. 2007; M. Sarzi et al. 2007) have concluded that in 30%–50% of the cases, the AGN is associated with young stellar populations (i.e., older than a few 100 Myr). However, this could be due to the fact that both AGN and starbursts require gas to fuel them, and does not necessarily imply a causal relation. For example, the color and morphology of low-redshift ($z < 0.3$) quasar host galaxies are not significantly different from those of normal (nonactive) galaxies (D. Bettoni et al. 2015), suggesting that nuclear activity does not affect the global properties of galaxies. Literature results regarding the AGN-starburst connection are controversial. It is yet unclear whether AGN activity occurs together with star formation (N. Kawakatu & K. Wada 2008), follows it during a post-starburst phase (R. I. Davies et al. 2007; R. A. Riffel et al. 2009; R. Riffel et al. 2022), or there is no association with recent star formation (M. Sarzi et al. 2007). The observational situation is ambiguous, with several studies showing evidence for quenching (M. J. Page et al. 2012; A. J. Barger et al. 2015; T. T. Shimizu et al. 2015; J.-J. Jin et al. 2018; A. Stemo et al. 2020), enhanced star formation (D. Lutz et al. 2010; J. R. Mullaney et al. 2012; P. Santini et al. 2012; M. E. Jarvis et al. 2020; J. Shangguan et al. 2020a; Y. Xie et al. 2021;

L. Koutoulidis et al. 2022), or no significant effect (C. M. Harrison et al. 2012; D. J. Rosario et al. 2012; B. Husemann et al. 2014; F. Stanley et al. 2015, 2017; H. Suh et al. 2017; J.-H. Woo et al. 2017; I. Smirnova-Pinchukova et al. 2022). One possibility is that these discrepancies reflect the different samples of AGN, the choice of comparison galaxies, and even evolutionary effects within the host galaxy population as a function of redshift. Similarly, earlier claims have been made that AGN hosts are dominated by old stellar populations (R. J. McLure et al. 1999; L. A. Nolan et al. 2001) and that they contain younger stars (G. Kauffmann et al. 2003; J.-J. Jin et al. 2018). On the one hand, we expect that AGN should accelerate quenching (J. Gofford et al. 2015; P. F. Hopkins et al. 2016), but this may also take place over longer timescales (S. B. Rembold et al. 2017; S. F. Sánchez et al. 2018). It is possible that these conflicting results reflect the influence of selection effects, different environments, and disparate methods to derive star formation histories (SFHs) for AGN host galaxies and the comparison systems. In A. W. Graham et al. (2024), mergers drive morphological transformation, not AGN feedback per se.

With this in mind, in this study, we set out to compare the star formation properties of a sample of Type I AGN hosts and of a comparison sample of normal (nonactive or without quasar activity) galaxies (CSNG) selected within the same volume. The samples are matched in the stellar mass distribution and redshift. Our purpose is to compare the SFHs of AGN host galaxies and those of normal galaxies to understand the role of AGN activity in shaping the stellar populations and SFHs of galaxies. We used the catalog of low-redshift Type I quasars by C. F. Wethers et al. (2022), which assembled all known Type I quasars from the recent compilation of quasar catalogs in C. Gattano et al. (2018) within the three equatorial fields of the Galaxy and Mass Assembly (GAMA) spectroscopic survey (J. Liske et al. 2015; S. P. Driver et al. 2018, 2022). We also select 200 sets of normal galaxies with the same redshift and mass distribution as the quasars to act as a comparison sample. This should lessen many of the selection effects that affect previous studies (such as any possible evolutionary issues, for example, since all objects are observed at the same epoch within a few hundred Myr). The star formation properties for CSNG are pulled from the GAMA archive. For quasar hosts, we use the CIGALE spectral energy distribution (SED) analysis tool to derive estimates of star formation properties, employing the most up-to-date AGN model available.

The structure of this paper is as follows: In Section 2 we discuss the data samples and the property estimates pulled from various archival databases. In Section 3, we detail how we estimate stellar population parameters for the quasar host galaxies. In Section 4 we present our main results, comparing star formation rates (SFRs) and SFHs for AGN hosts and normal galaxies. We discuss our results in Section 5 in the light of models for AGN formation and feedback. Conclusions are presented in Section 6. Throughout this paper, we use the cosmological parameters from Planck Collaboration et al. (2020).

2. The Samples

Based on the data provided by the GAMA spectroscopic survey, first, the sample of quasars is assembled (Section 2.1), consisting of all known bright low-z Type I AGN that are located in the GAMA equatorial footprint. Observational properties of the quasar sample are given in Section 2.2, based on the existing surveys. Since there are many different types of AGN, these additional properties are given to indicate that, overall, the quasar sample in this work consists of typical low-redshift Type I AGN; our quasar sample is representative of that group of quasars.

Next, we extract the comparison sample of normal galaxies or CSNG (Section 2.3) to match the quasar sample. The CSNG serves as a control group. GAMA database ancillary products include estimates of SFRs for the comparison galaxies in the control group, as described in Section 2.4, and we use those in this work.

2.1. Low-redshift Quasar Sample

The low-redshift quasar sample is comprised of all known bright Type I AGN located within the equatorial volumes covered by the GAMA survey, and is taken from C. F. Wethers et al. (2022). The quasar catalog C. F. Wethers et al. (2022) is made up of 205 low-z Type I quasars. We briefly summarize how this sample of quasars was constructed: a full description is given in C. F. Wethers et al. (2022).

C. F. Wethers et al. (2022) catalog of quasars was drawn from version 4 of the Large Quasar Astrometric Catalog (LQAC-4; C. Gattano et al. 2018). LQAC-4 is the most homogeneous and complete quasar catalog to date, crossmatching 12 independent quasar surveys, alongside the M. P. Véron-Cetty & P. Véron (2010) quasar catalog. LQAC-4 provides *ubvgrizJK*-band photometry, radio fluxes (at 1.4 GHz, 2.3 GHz, 5.0 GHz, 8.4 GHz, 24 GHz), and spectroscopic redshifts.

The following selection constraints were applied by C. F. Wethers et al. (2022) to the objects in the LQAC-4 catalog:

1. The quasars had to be within the three equatorial areas of the GAMA survey (MagPhys Data Management Unit; DMU).
2. The redshift range was set to $0.1 < z < 0.35$, a redshift interval corresponding to a timescale of around 1 Gyr. At this redshift range, the GAMA survey probes the largest volume with the highest completeness. We note that within this relatively short time frame, any possible evolutionary effects are likely to be less relevant.
3. The objects had to be brighter than $r = 19.8$. This selection criterion for apparent brightness was also imposed, since GAMA is complete beyond 99% at $r < 19.8$ mag (Sloan Digital Sky Survey (SDSS) photometry).

After the above selection procedure, C. F. Wethers et al. (2022) proceeded to positionally match the LQAC-4 quasars to a GAMA target within 5″: 90% of the LQAC-4 quasars were identified as GAMA targets. The final quasar sample of 205 objects is also available as a VizieR catalog, which includes the GAMA ID, coordinates, and redshifts for each quasar (C. F. Wethers et al. 2022).

All of these quasars also fulfill the criteria for inclusion in the SDSS DR12 catalog of Type I quasars (I. Pâris et al. 2018). The environment around this sample of quasars has been studied at different scales (C. F. Wethers et al. 2022; M. B. Stone et al. 2023). Crucially, by selecting bright quasars within the GAMA equatorial footprint, we were able to utilize the full GAMA spectroscopic survey of several hundred

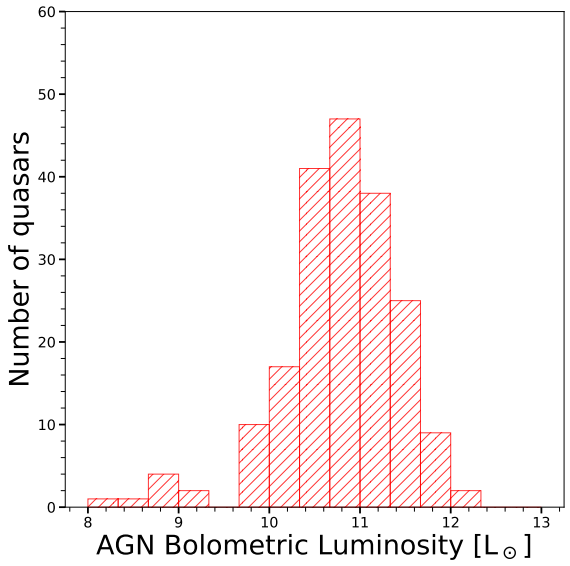

(a)

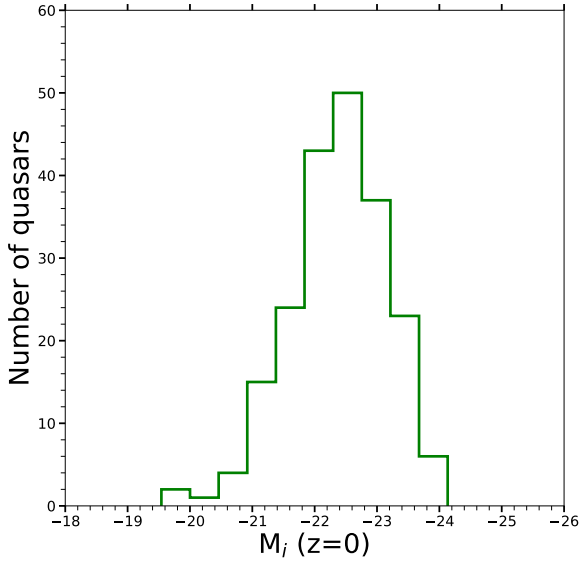

(b)

Figure 1. (a) Distribution of bolometric luminosities for quasars derived from CIGALE fits. This excludes eight quasars (3.9% of the quasar sample) where CIGALE did not return a quasar luminosity. (b) Distribution of absolute SDSS *i*-band magnitude (*k*-corrected and extinction corrected based on GAMA survey data).

thousand galaxies within the same patch of the sky to construct the control sample of normal galaxies for comparison, as described in the section (Section 2.3).

2.2. Quasar Sample Properties

Here we consider the luminosity distribution (Section 2.2.1) and spectral types of quasars (Section 2.2.2) in our GAMA sample. We compare our sample to the quasars from large surveys in the literature. This comparison confirms that our quasar sample (which is constrained to the GAMA equatorial volume) consists of typical quasars. (The star formation properties of the quasar sample are discussed in the next section, Section 3).

Table 1
Categories of Quasars Based on Spectral Type in This Work versus the Literature Quasar Catalog[a]

Category	This Work	M. P. Véron-Cetty & P. Véron (2010)
	$N = 205$	$N = 9586$
(1)	(2)	(3)
S1	192 (94%)	9353 (97%)
S2	13 (6%)	0
S3 (LINER)	0	233 (3%)

Note. Column (1): quasar classification category. Column (2): category fractions of the full quasar sample used in this work. Column (3): category fractions of quasars from the literature.
[a] M. P. Véron-Cetty & P. Véron (2010).

2.2.1. Luminosity of the Quasar Sample

The AGN bolometric luminosity and the distribution of the absolute luminosities in the *i* band are shown in Figure 1. The bolometric luminosity is characteristic of low to intermediate-luminosity objects. This is not surprising, as powerful quasars will be rare within these relatively small volumes.

2.2.2. Classification of Quasars

We classified *by eye* the optical spectra of quasars using the spectra in the GAMA archive. We used three broad categories: quasars with at least one broad line (Seyfert 1 or S1), quasars with narrow lines (Seyfert 2 or S2), and systems with low-ionization nuclear emission-line regions (LINERs), following the classification scheme of the M. P. Véron-Cetty & P. Véron (2010) catalog. The results are presented in Table 1. We further compared our visual classification with M. P. Véron-Cetty & P. Véron (2010) catalog classifications, and found them to be mostly consistent with each other.

If no classification was given in M. P. Véron-Cetty & P. Véron (2010), then, when possible, for these rare cases, we adopted classifications from more recent catalogs in the VizieR service (e.g., S. Rakshit et al. 2017). A small number of quasars, however, did not have any spectral classification in the existing catalogs, and we used the visual classifications as the final determination.

Most of our galaxies are Seyfert 1 with typical broad emission lines. The mean redshift of the quasar sample is $z = 0.224 \pm 0.072$, while the mean absolute magnitude is $M_i = -22.38 \pm 0.77$. Compared to the previous low-redshift study of Type I quasars by R. Falomo et al. (2014), our sample of quasars also probes lower brightness AGN, due to the different cuts imposed by quasar catalogs (e.g., SDSS quasar catalog) available at the time. Our sample is essentially consistent with that of M. P. Véron-Cetty & P. Véron (2010), as shown in Table 1, and appears to be representative of the average population of AGN within this redshift range ($0.1 < z < 0.35$).

2.3. Comparison Sample of Normal Galaxies

It is important to compare any results from our quasar sample with a control sample of normal galaxies, in order to ascertain that the observed characteristics are indeed unique to quasar host galaxies (as discussed previously, e.g., K. Karhunen et al. 2014). The GAMA spectroscopic survey database is where the

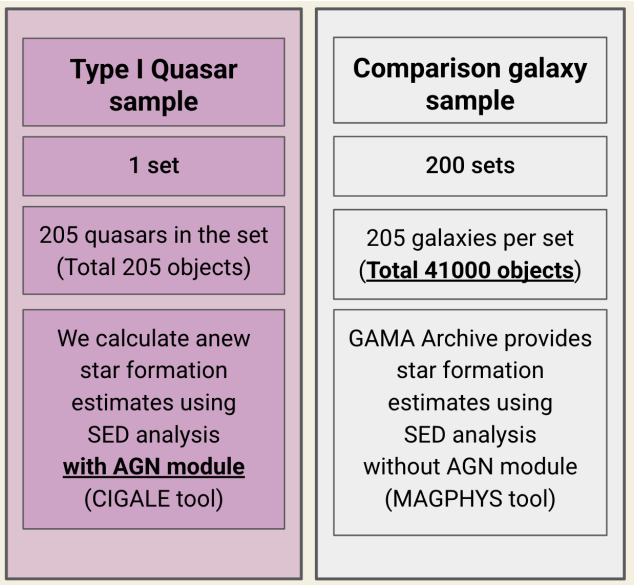

Figure 2. Our quasar sample consists of 205 objects. Our CSNG is constructed using the GAMA archival data and consists of 200 sets, where each set has 205 normal galaxies. The CSNG is from the same volume as the quasar sample. The redshift and stellar mass properties are matched to the quasar sample as well (Figure 3). The quasar sample is obtained from C. F. Wethers et al. (2022), and the CSNG is obtained from M. B. Stone et al. (2023).

normal galaxies for CSNG are selected, because in addition to the robust redshifts, the GAMA archive provides estimates of physical properties (S. P. Driver et al. 2022). Thus, the match between the active and normal galaxies is robust, since both the redshift and the physical properties are matched between the two samples.

The CSNG for our quasar sample is obtained from M. B. Stone et al. (2023) and consists of 200 sets of normal galaxies (Figure 2). All galaxies were extracted from the GAMA spectroscopic survey (MagPhys DMU). Each set of normal galaxies has:

1. 205 normal galaxies, as in our quasar sample,
2. Is within the same volume as the quasar sample, and
3. Is matched in redshift and stellar mass to the quasar sample (Figure 3).

Note that the CSNG does not have restrictions on the SFRs, and control galaxies range from star-forming to objects with low SFR activity (similar to D. Bettoni et al. 2015).

The matching method used by M. B. Stone et al. (2023) to build these comparison sets of normal galaxies was based on a Monte Carlo realization of samples technique, and this method was first presented in C. F. Wethers et al. (2022). Briefly, for each quasar, a randomly selected galaxy having the same redshift within $\Delta z = 0.01$ and the same stellar mass within 0.1 dex is selected as a normal counterpart. This process is repeated for all quasars until a comparison set of 205 GAMA non-AGN galaxies is defined. In the same way, 200 such comparison sets were created. As shown in Figure 3, this results in closely matched samples of galaxies and quasars, as checked both by the Kolmogorov–Smirnov and the Anderson–Darling statistical tests.

2.4. GAMA Archive Star Formation Properties for CSNG

The star formation properties for normal galaxies were retrieved from the archives of the GAMA database. GAMA

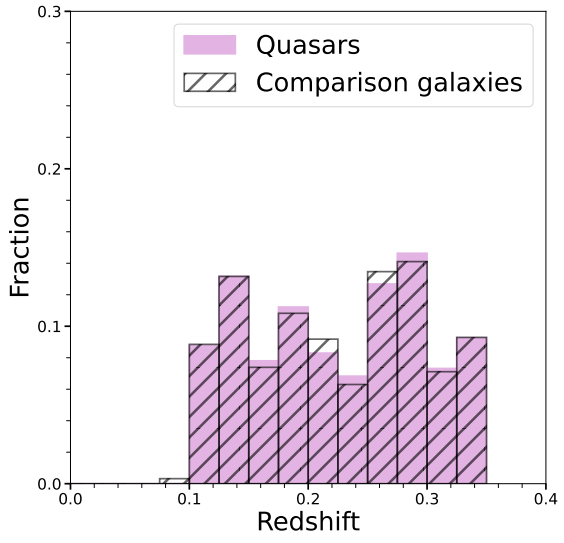

(a)

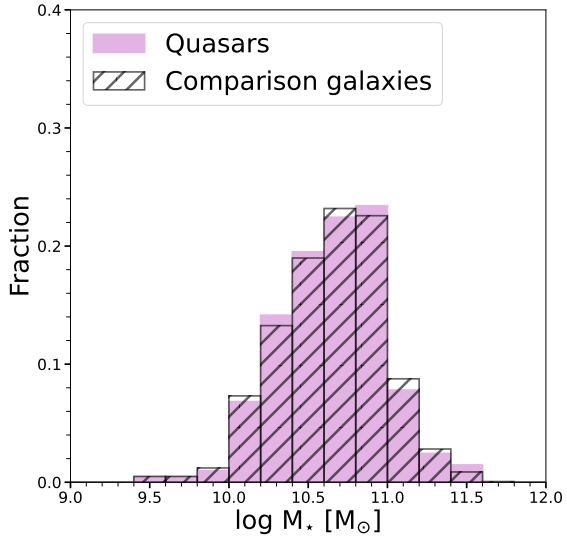

(b)

Figure 3. (a) Redshift and (b) stellar mass distributions of quasars and comparison galaxies (reproduction of Figure 1 from M. B. Stone et al. 2023). The two-sample Kolmogorov–Smirnov test (p-value > 0.99) shows that there is no significant difference statistically between the matched normal galaxies sample and the quasar sample (same result with the Anderson–Darling test).

derives estimates for the stellar population properties (such as SFRs and SFHs) by fitting the SEDs of galaxies with the MAGPHYS tool (E. da Cunha et al. 2008; E. da Cunha & S. Charlot 2011). The SEDs used by GAMA are based on the 21−band fluxes for the equatorial survey regions (Table 2), covering wavelengths from far-UV to far-infrared (Lambdar-Photometry DMU; S. P. Driver et al. 2016; A. H. Wright et al. 2016).

The SED-based estimates are drawn from within the MagPhys DMU of the GAMA survey (S. P. Driver et al. 2022). We extracted the following properties from the MagPhys DMU for CSNG: stellar masses, SFRs, and SFRs averaged over the past 10, 100, 1000, and 2000 Myr, plus the estimates for the averaged SFR for older stellar populations.

Table 2
GAMA Spectroscopic Survey Photometry Bands

Bands	Survey
Far-UV, near-UV	GALEX (D. C. Martin et al. 2005)
u, *g*, *r*, *i*, *z*	SDSS Data Release 7 (DR7) K. N. Abazajian et al. 2009
Z, *Y*, *J*, *H*, *Ks*	VIKING (A. Edge et al. 2013)
W1–W4, ∼2–30 μm	WISE All-Sky DR (E. L. Wright et al. 2010)
100 μm, 160 μm	Herschel Astrophysical Terahertz Large Area Survey (S. Eales et al. 2010) PACS
250 μm, 350 μm, 500 μm	Herschel SPIRE

Note. Column (1): GAMA LambdarPhotometry DMU photometry bands. Column (2): Source surveys.

While there are estimates in the GAMA archive also for our quasar sample, we perform a separate analysis to estimate the star formation properties for quasar hosts, in order to include the most up-to-date SED models which account for the presence and contribution of the AGN, as described in the next section (Section 3). Additionally, we perform similar CIGALE fits for comparison on a representative subsample of CSNG, described in (Section 3.3), to make sure that the comparison between the quasar hosts and normal galaxies is homogeneous.

3. SFR and SFH Estimates for Quasar Hosts

In this section, we present the necessity and justification for rederiving the estimates for star formation properties for the quasar sample with the CIGALE SED tool (Section 3.1). Then we present the details on how the CIGALE SED fits were setup for the quasar hosts (Section 3.2). We describe a few comparison tests between CIGALE and MAGPHYS (Section 3.3). In particular, an additional check was performed for a single set of normal galaxies from the control group. We further introduce a statistical correction between the two SFR estimators. For completeness, a brief discussion is included to describe the underlying assumptions, such as the initial mass function (IMF) for both codes.

3.1. CIGALE AGN Module

Accounting for the AGN contribution is necessary in assessing the quasar host star formation properties; lack of such consideration results in overestimation of the parameters. Thus, we adopt the CIGALE SED fitting code to analyze all objects in our quasar sample, because CIGALE allows the inclusion of an AGN component in SED fits (D. Burgarella et al. 2005; S. Noll et al. 2009; M. Boquien et al. 2019; G. Yang et al. 2022).

To account for AGN contribution, we chose the most up-to-date AGN model, the SKIRTOR module. The SKIRTOR module has a realistic two-phase torus model. Additionally, the SKIRTOR AGN module covers the UV–IR range, which matches the GAMA photometry interval.

For quasar host galaxies in our sample, it was not possible to use the star formation estimates from the available GAMA archive because the GAMA SED fits did not include the AGN contribution. In addition, it was not possible to use the MAGPHYS SED fitting code, as in the GAMA archive, because that code did not have models for the AGN contribution. The MAGPHYS team started developing this capability recently (J. S. da Cunha et al. 2026, in preparation). We discuss the differences between the codes later in this section.

The separation of AGN from galaxy light has been treated and tested by the CIGALE team (M. Boquien et al. 2019; C. Yang et al. 2019; G. Yang et al. 2022), including for the case of the SDSS Type I quasars, i.e., the same category of quasars as in this work. Numerous later studies used CIGALE to tackle the AGN contribution in SED analysis and confirm that this method is effective and reliable both at low and at high redshifts (e.g., C. Circosta et al. 2018; G. Mountrichas et al. 2022a, 2022b; I. Georgantopoulos et al. 2023). This is generally true even for the most luminous quasars, although these are not generally present within the GAMA volume (see Section 2.2).

We stress that for normal galaxies, the estimates of SFR and similar quantities are published in GAMA archives, as described in Section 2.4. As there is no need to include the AGN component in SED fits for normal galaxies, the fits provided by GAMA are satisfactory; it is not necessary to rederive them again with CIGALE (which would be a computationally intensive task as the comparison sample consists of more than 40,000 objects). Nevertheless, we did run comparison tests with CIGALE for a representative subsample of control galaxies, described in Section 3.3. Furthermore, as presented in that same section, extensive comparative analysis of both codes by L. K. Hunt et al. (2019) asserts that the resultant estimates from both codes are similar and equally reliable.

3.2. CIGALE Parameters for the Quasar SED Fits

We use the same multiband data from the GAMA Lambdar catalog for building CIGALE fits. We used version 2022.1 of CIGALE, which is Python based.

CIGALE uses a series of modules for SFH, single stellar population (SSP), and other contributions to build the final SED of a galaxy (M. Boquien et al. 2019). The chosen modules, parameters, and their values for the quasar hosts with AGN components are given in Table 3. Neither X-ray nor radio data are present in the GAMA survey archive, so these modules are not included.

We assume the *delayed* SFH scenario with a star formation burst (M. Boquien et al. 2019; G. Yang et al. 2022). The library of SSP templates is from G. Bruzual & S. Charlot (2003), allowing for the construction of the stellar emission part of the SED from the galaxy host. We use the Chabrier IMF (G. Chabrier 2003) and assume solar metallicity ($Z = 0.02$) following L. Ciesla et al. (2015). The stellar emission is attenuated by applying the D. Calzetti et al. (2000) dust extinction law.

The contribution due to dust heating by the stellar component is modeled by adopting the D. A. Dale et al. (2014) dust templates with parameter values as in L. Ciesla et al. (2015). To include the non-stellar emission contribution from the AGN, we use the newer AGN templates—the SKIRTOR templates (M. Stalevski et al. 2012, 2016), but only for Type I quasars, since our sample only contains Type I AGN. For the input parameters, we use the suggestions from G. Yang et al. (2022) for the SDSS quasar case.

For eight objects, the SED fit had zero AGN luminosity; however, this does not affect the conclusions of this work. We do not force the SED fit to choose quasar models, so in these eight cases, the best fit found in the library was not the SED of

Table 3
Model Parameters for SED Fitting with CIGALE

Module and Parameter (Symbol)	References and Values
SFH	*Delayed SFH with an optional recent burst*
Age of the main population (Myr)	3000, 5000, 7000, 8000, 9000, 10,000
e-folding time of the main population (Myr), $\tau_{\rm main}$	1000, 3000, 5000, 8000, 10,000
Age of the recent burst (Myr)	50, 20,000 (continuous SFH)
e-folding time of the burst (Myr)	50, 500
Burst mass fraction	0.0, 0.1
SSP	G. Bruzual & S. Charlot (2003)
IMF	G. Chabrier (2003)
Metallicity (Z)	0.02 (Solar)
Galactic dust attenuation	*D. Calzetti (2000) attenuation law*
Color excess of nebular lines	0.1, 0.2, 0.3, 0.4, 0.5, 0.6
Reduction factor	0.44
Slope of the power law	−0.2, 0.0
Galactic dust emission	D. A. Dale et al. (2014)
Alpha slope	2.0
AGN (UV to IR)	*SKIRTOR* (M. Stalevski et al. 2012, 2016)
Viewing Angle	30° (Type I)
Delta	−1, −0.9, −0.8, −0.7, −0.6, −0.5, −0.4, −0.3, −0.2, −0.1, 0.1, 0.6
AGN fraction	0.0, 0.01, 0.1, 0.2, 0.3, 0.4, 0.5, 0.6, 0.7, 0.8, 0.9, 0.99
$E(B-V)$ (magnitudes)	0., 0.05, 0.1, 0.2, 0.4, 0.6
Extinction law of polar dust	Small Magellanic Cloud

Note. Column (1): list of parameters in each module of the CIGALE SED tool used in this work. Column (2): parameter values adopted in our SED analysis with the CIGALE tool. The AGN component (SKIRTOR) was included only for quasar fits. For further details on the parameters, see the CIGALE manual and M. Boquien et al. (2019), G. Yang et al. (2022).

a quasar. We chose not to add additional parameters because it is not possible to get a perfect fit for every single quasar in the sample; we employ a single set of parameters to fit SEDs for the full quasar sample. Enlarging the parameter space may result in overfitting and in different sets of misfits. The parameter grid size is a balance between fitting well as many quasars as possible in the sample and avoiding overfitting and high computational pressure. The quality of fits is primarily limited by the uncertainties in the input photometry and by the content of the CIGALE library of SEDs.

3.3. Comparing Our CIGALE Estimates to GAMA Data

We perform two comparison tests to check how the estimates based on the CIGALE fits compare to the archival data from the GAMA spectroscopic survey (Table 4). We perform both a test for the quasar sample (test A) and a test for the CSNG (test B).

3.3.1. Test A: Check the Effect of AGN Contribution to the SED Fits

In test A, we compare our CIGALE results with AGN components to the archival GAMA data for quasar hosts, which did not include the AGN contribution. GAMA archive is based on MAGPHYS SED fits, as noted previously. We show one example of a quasar in our sample, analyzed both with AGN and without AGN, in Figure 4. Comparisons for the SFR, specific SFR (sSFR), and stellar mass are given in Figure 5. Not surprisingly, MAGPHYS tends to overestimate the SFRs (ignoring the AGN component) while the derived stellar masses are comparable. Thus, this test result shows that it is important to consider the AGN component when performing SED-based analysis to derive properties for quasar hosts.

3.3.2. Test B: Check the Agreement between Two Codes for CSNG

It is expected that for normal galaxies, the estimates of properties should not depend on which SED tool is used, CIGALE or MAGPHYS. Thus, next, in test B, we considered the normal galaxies and compared the results of CIGALE fits (with no AGN component) to GAMA archive data (based on MAGPHYS). This test was done for *one* CSNG set. Rather than running CIGALE on thousands of GAMA galaxies, we selected a representative subsample, matching the quasar sample (same number of objects, same distribution in redshift and mass, same survey volume). We perform Test B to make sure that the comparison between quasars and nonactive galaxies is homogeneous. The test result for SFR, sSFR, and stellar masses is given in Figure 6.

The SED fits with CIGALE for normal galaxies were setup identically to the quasar hosts, with the exception of the AGN module; the AGN component was not included. Table 3 gives the list of all parameters for the CIGALE fits for normal galaxies as well. The expectation in test B is that it does not matter which SED software is employed to estimate SFRs, so the expected output should result in similar results. Indeed, this is what we observe, as shown in Figure 6. For the vast majority of normal galaxies, there is virtually no difference between the two estimates with two different codes. Only for a few objects with extremely low SFR values, the differences between the two estimates deviate from zero. However, both algorithms suffer from poor performance at this extreme regime in SFR, and it is not possible to say that one evaluates the extremely low SFR values more precisely. As the number of objects in that regime is small, our results and conclusions are not affected.

MAGPHYS and CIGALE also provide estimates for the SFR averaged over the past 10 and 100 Myr. MAGPHYS also provides estimates over the past 1000 and 2000 Myr. Both codes measure the contributions from old stellar populations. In Figures 7 and 8 we compare the results from CIGALE and MAGPHYS for the SFR averaged over the past 10 and 100 Myr. Similar to SFR estimates, we find that MAGPHYS overestimates SFR averages over the past 10 Myr but less so when averaged over the past 100 Myr.

In this work, for quasar host galaxies, we will use CIGALE-derived values for SFR, sSFR, stellar masses, and the SFR averaged over 10 and 100 Myr, as well as the contribution from older stellar populations. We will use the MAGPHYS values for the SFR averaged over the past 1000 and 2000 Myr as CIGALE does not provide these values. However, given the relative similarity of CIGALE and MAGPHYS results for the SFR averaged over the past 100 Myr and the older stellar populations, we regard this choice as permissible.

A thorough comparison of the results of both codes has been carried out by L. K. Hunt et al. (2019), who also present a tabular version of similarities and differences between codes (e.g., assumptions in fits are given in their Table 1). Their results show that both codes yield similar estimates of parameters such as stellar masses, SFRs, and SFHs within

Table 4
Comparison Tests of Star Formation Properties between the Derivations with CIGALE Fits in This Work and GAMA Archival Data

Test ID (1)	Population (2)	Comparison Description (3)	CIGALE AGN Module (4)	Figure References (5)
A	Quasar sample	CIGALE fits to GAMA data	Included	5, 7
B	A single set of galaxies from CSNG	CIGALE fits to GAMA data	Not included	6, 8

Note. Column (1): test ID. Column (2): population compared. Column (3): AGN module inclusion in CIGALE fits. (Note that in all cases, GAMA archival data does not include AGN contribution to the SED fits.) Column (4): figures with test outcome.

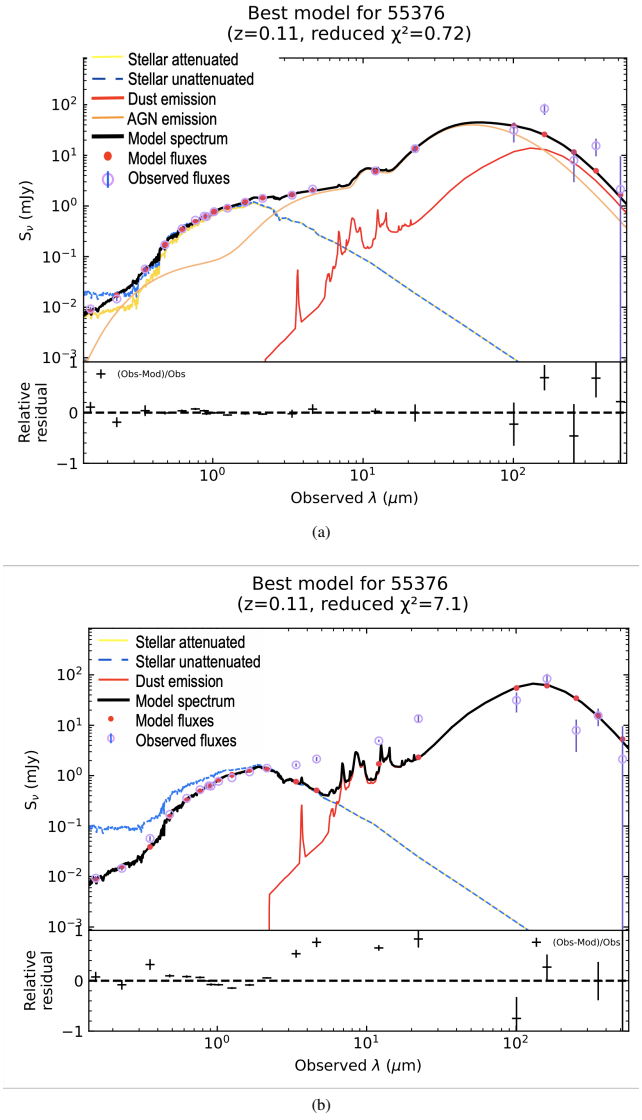

Figure 4. SED analysis result with CIGALE for one quasar in our sample. (a) The top panel shows the result, which includes AGN taken into consideration. AGN emission is represented by the solid orange line. (b) The bottom panel shows the best model without the inclusion of the AGN module. Note that the reduced χ^2 value is much lower when AGN is considered, indicating a better fit.

0.1 dex, i.e., within the typical photometric errors. This is confirmed in our comparison of MAGPHYS and CIGALE estimates of these parameters for a single set of normal galaxies, i.e., from test B. As in L. K. Hunt et al. (2019), we find a tendency for CIGALE to overestimate SFRs for very low star formation levels (also see the more recent comparison for GAMAnear galaxies by E. D. Paspaliaris et al. 2023).

We observe that in our dataset, both methods also appear to yield similar results. The average differences $\Delta\mathrm{SFR}_{\mathrm{CIGALE-MAGPHYS}}$, $\Delta\mathrm{sSFR}_{\mathrm{CIGALE-MAGPHYS}}$, and $\Delta\mathrm{mass}_{\mathrm{CIGALE-MAGPHYS}}$ are (0.03, 0.00, and 0.03). Almost all of the comparison normal galaxies lie between 0.2 dex of the CIGALE value in SFR, sSFR, and stellar mass (Figure 6). The similarity between SFR, sSFR, and stellar mass estimates based on MAGPHYS/CIGALE fits is further highlighted by the median differences of the property per 1 dex bin in each case (red dots in Figure 6). There is a trend for CIGALE to overestimate SFR at low values, which is typical of quiescent galaxies (see L. K. Hunt et al. 2019). The differences between values from CIGALE and MAGPHYS are significantly smaller than the histogram bins we use in subsequent figures. In the remainder of the analysis, we will use MAGPHYS values for normal galaxies in the CSNG, as these estimates are already provided by the GAMA survey for all 200 sets of comparison galaxies (while running CIGALE is found to be computationally expensive).

3.3.3. Statistical Correction for SFR Values between CIGALE and MAGPHYS

In this work, two SFR estimators are used—one based on CIGALE for the quasar sample because it includes AGN contribution and the second one from the GAMA survey based on MAGPHYS for the control sample. We introduce a statistical correction to bring the CIGALE values to the MAGPHYS baseline. Thus, any discrepancies between the two estimators are removed and consequently do not affect the results. Any systematic errors are also reduced.

To obtain the calibration function, we fit a Chebyshev polynomial to the SFR parameter offsets versus its CIGALE estimate, which is then used to obtain the corrected parameter value,

$$\log_{10} X_{\mathrm{corr}} = \log_{10} X_{\mathrm{CIGALE}} - f_{\mathrm{Cheb}}(\log_{10} X_{\mathrm{CIGALE}}) , \qquad (1)$$

where X stands for any SFR parameter, f is the statistical correction function for the offsets, and X_{corr} is the parameter value corrected to the MAGPHYS baseline. This is applied to all SFR parameters of the quasar sample: SFR, sSFR, and time-averaged SFR. This correction is minor and does not substantially change the results. The analysis uses the code described in the software section (M. B. Stone 2025c,2025d).

3.3.4. Main Ingoing Assumptions for CIGALE and MAGPHYS

For completeness, we highlight the main assumptions and sources of uncertainties. Uncertainties in the SED estimates arise from the input photometry data. There is no difference in input for the models between MAGPHYS and CIGALE in this work. GAMA MAGPHYS SED fits are based on LAMBDAR photometry. We used the same panchromatic data from

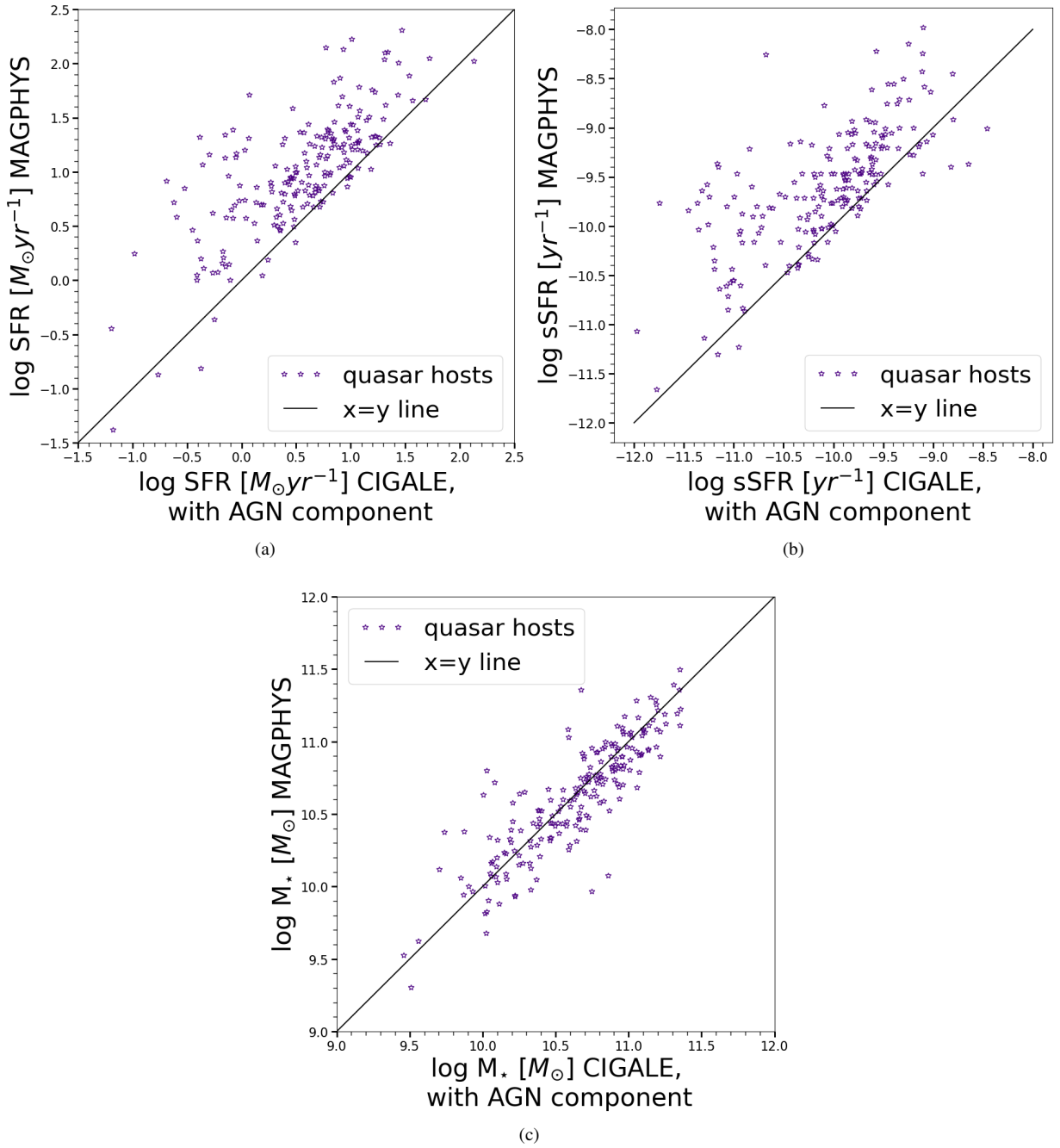

Figure 5. Results for comparison test A. Comparison between the GAMA archival data (MAGPHYS SED fitting results with no AGN component) and our CIGALE SED fitting results (including an AGN component) for (a) SFR, (b) sSFR, and (c) stellar mass for the sample of quasar host galaxies. The SFR and sSFR estimates differ significantly when an AGN contribution is included in the SED analysis, prompting us to derive anew the star formation property estimates for the quasar sample.

LAMBDAR photometry for CIGALE fits. The UV and IR survey photometry data in GAMA often have larger associated uncertainties compared to the measurements within the optical wavelengths. GAMA SED fits are based on a parameter space chosen to cover all the galaxies in the survey, not just the bright and low-z galaxies. As we are looking only at a subset of galaxies from the GAMA survey, our parameter space with SED fits with CIGALE performed here is tailored.

Both MAGPHYS and CIGALE adopt a computationally efficient energy balance approach to derive SEDs coupled with a Bayesian estimator to recover the full posterior probability distribution of galaxy physical parameters. The application of MAGPHYS to GAMA data is described in S. P. Driver et al. (2018). Note that GAMA archival fits were performed on the full GAMA catalog, not focused on the low-z sample of bright galaxies. There are uncertainties associated with models in each module of the SED program (e.g., C. Conroy 2013), which need to be remembered when interpreting results. Both codes (as well as others) rely on a given SFH defined by an assumed IMF (G. Chabrier 2003 for both codes) applied to a matrix of single-age stellar populations (G. Bruzual & S. Charlot 2003 for both codes), see Table 5. However, CIGALE adopts a single (solar) metallicity and an SFH based on a delayed parameterization approach as

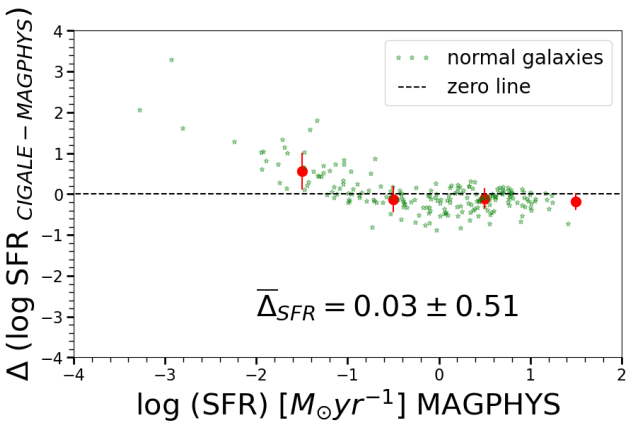

(a)

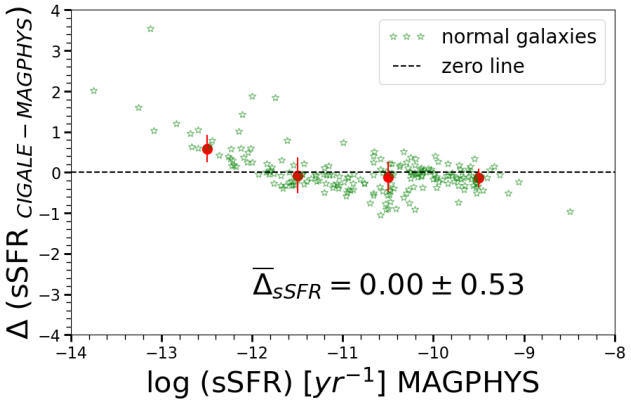

(b)

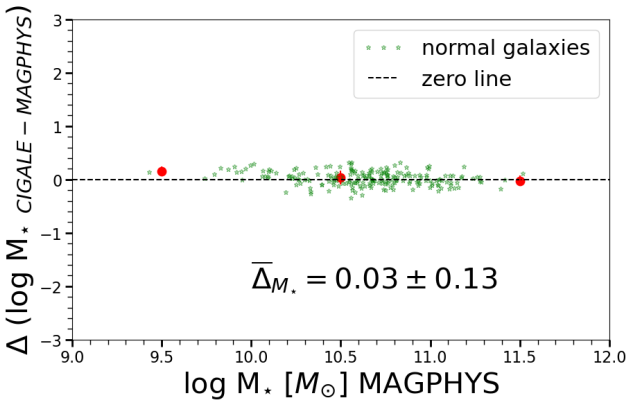

(c)

Figure 6. Results for comparison test B. Differences (Δ) comparing the MAGPHYS and CIGALE SED fitting results (without AGN component) for (a) SFR, (b) sSFR, and (c) stellar mass for normal galaxies. The red-filled circles represent the median log difference in each 1 dex bin of SFR between the two estimators, excluding the bins with small number statistics. Error bars reflect the standard deviation in that bin. We remark that in all half dex intervals the only difference between CIGALE and MAGPHYS is a small (on the order of 0.01 dex) offset with no particular trend, except at very low SFR, where essentially all models can yield different results based on small differences in input parameters.

described by L. Ciesla et al. (2015), whereas MAGPHYS adopts an exponentially declining SFH, with SSPs having varying metallicities with random bursts to mimic realistic histories. However, there is no AGN module in MAGPHYS. The MAGPHYS research team is developing the inclusion of AGN, but it is not yet finished. We stress, however, that despite the underlying assumptions, the SED-based analysis generally produces good estimates of stellar population parameters for galaxies in general, as described in the relevant documentation papers for both codes.

Previous studies, such as those of M. B. Stone et al. (2021) and D. Bettoni et al. (2023), were able to assess only a few parameters through optical spectroscopy, such as SFR, sSFR, and stellar mass estimates for quasar hosts based on emission line analysis. The SED analysis provides a larger set of parameter estimates, which include SFH parameters and AGN-related parameters. While future surveys are planned to get spectroscopy data for a large number of quasars, currently, the GAMA survey already holds the photometry data for SED-based analysis.

4. Results

In this section, we present the distributions of star formation properties of the low-z quasar sample, obtained through the CIGALE SED tool (Section 4.1). Moreover, various SFH parameters are compared between the quasar sample and the CSNG (Section 4.2).

4.1. Comparing the SFR Distribution of the Quasar Sample with Normal Galaxies

To demonstrate how the SFR of quasar hosts compares to that of normal galaxies, we map in Figure 9 (right) the stellar mass versus sSFR for the sample of quasar host galaxies and for a Monte Carlo realization of 200 samples of 205 normal galaxies. The majority of quasars, 80%, lie above the cutoff between star-forming galaxies (SFGs) and passive galaxies, $\log(\mathrm{sSFR}) = -10.8 \quad M_\odot\ \mathrm{yr}^{-1}$. (Note that ∼15% of the quasar sample is radio-loud using a limit of 1 mJy for 20 cm emission.)

The comparison galaxies are chosen to lie in the same volume, have the same stellar mass and redshift as the sample of quasar host galaxies. We further contrast the two samples in Figure 10, where we plot the histograms of SFR (a) and sSFR (b) for quasar host galaxies and the CSNG.

4.2. SFH Parameters of Quasar Hosts

SFH indicators, such as SFR averaged over 10, 100, 1000 and 2000 Myr can be employed to check how star formation evolves and compare the results with time intervals from quasar evolution models. CIGALE provides estimates of the SFR averaged over the past 10 and 100 Myr. MAGPHYS also provides estimates over the past 1000 and 2000 Myr but, unfortunately (as we can see in Figure 7), this neglects the influence of the quasar. In that figure, we see that the effect of the AGN is less important when averaged over longer epochs, so we also present MAGPHYS data (for SFR averaged over 1000 and 2000 Myr) with the caveat that these estimates may be affected by AGN light (i.e., over-estimated). This is shown in Figure 11.

Further information about the SFH is gleaned from the perspective of the old stellar population parameters. We present in Figure 12 the distributions of age of the oldest stars, as well as the stellar mass and luminosity of old stellar populations. The plots show no significant difference between CSNG and the quasar sample.

5. Discussion

We interpret the results disclosed in Section 4 here.

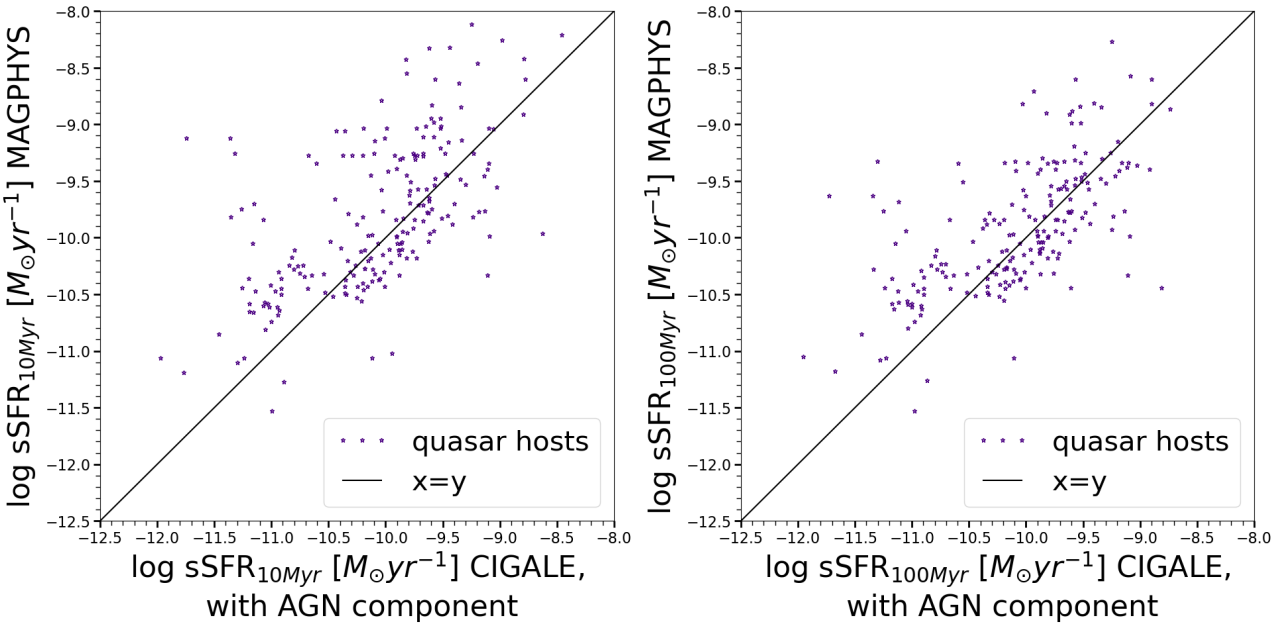

(a) (b)

Figure 7. Comparison between the MAGPHYS (no AGN component) and CIGALE (with AGN component) SED fitting results for sSFR averaged over the past (a) 10 and (b) 100 Myr, for quasar hosts (test A).

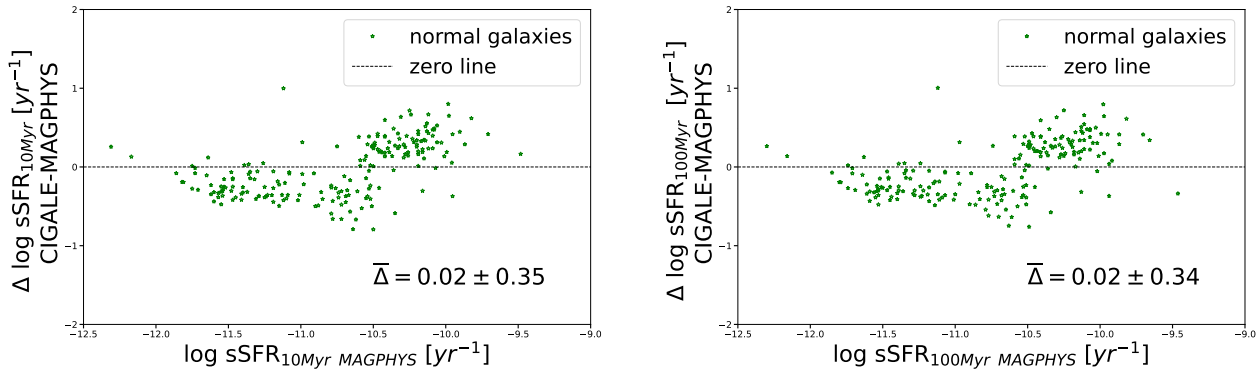

(a) (b)

Figure 8. Differences (Δ) between CIGALE and MAGPHYS estimates for normal galaxies (without AGN component) for sSFR averaged over the past (a) 10 and (b) 100 Myr (test B). The remark in the Figure 6 caption applies to these panels as well.

Table 5
Comparison of the Main Ingoing Assumptions between CIGALE Fits and GAMA Survey Fits with the MAGPHYS SED Code

Module (1)	MAGPHYS Fits in GAMA (S. P. Driver et al. 2018) (2)	Contrast with CIGALE Fits in This Study (3)
IMF	G. Chabrier (2003)	Same
SFH	Single (exponentially decaying) SFH	Different
SSP	BC03 models (G. Bruzual & S. Charlot 2003)	Same
Dust attenuation law	S. Charlot & S. M. Fall (2000)	Different
Metallicity	A wide range of values	A single value

Note. Column (1): name of the component module. Column (2): assumed law and/or parameter values from the GAMA archival data, which is based on the MAGPHYS SED tool. Column (3): comment on whether there are any differences when compared to the CIGALE SED fits performed in this work.

5.1. Quasar Host Galaxies are Mostly Star Forming

The distribution of quasar host galaxies in the stellar mass versus SFR (sSFR) plot (Figure 9) is broadly consistent with that of normal SFGs, with a smaller fraction lying in the green valley or just below in the quenched region. This can also be observed in the histograms shown in Figure 10. There are few to no quasars in the fully quenched region. However, the more quiescent objects can generally be seen to be more massive systems as in I. Smirnova-Pinchukova et al. (2022).

This confirms that quasar host galaxies are generally similar to normal SFGs and are less represented among the quiescent

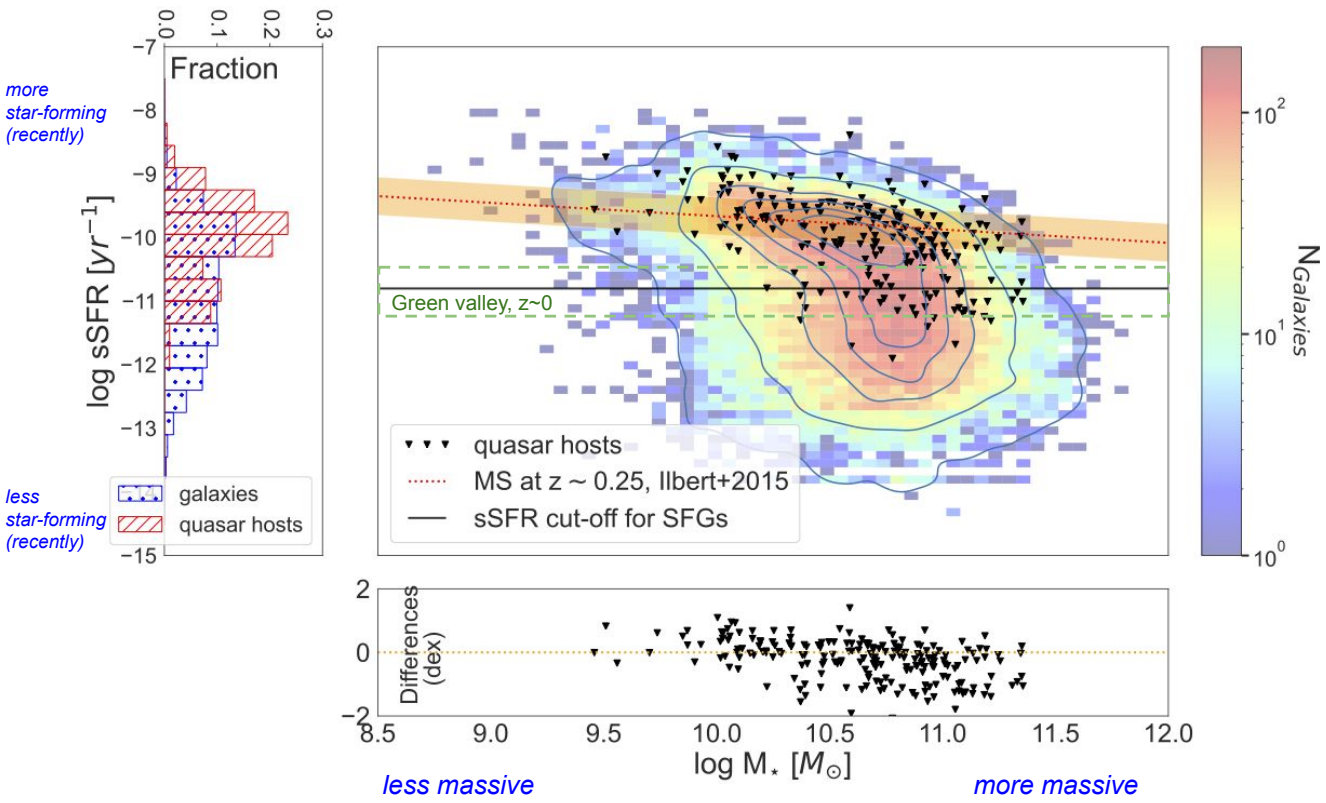

Figure 9. Top left: distribution of sSFR for quasars and comparison galaxies. Top right: stellar mass vs. sSFR for quasars (black triangles) and for comparison galaxies (contours and heatmap). The contour lines enclose 1/10/30/50/70/90% of comparison galaxies. The heatmap colors go from blue to red, corresponding to low to high values of comparison galaxy population counts, as indicated by the colorbar. The MS relation for SFGs from O. Ilbert et al. (2015) is given here in an orange dotted line, where the orange shaded area indicates the typical σ value of 0.3 dex (A. Katsianis et al. 2019). The black solid line indicates the cutoff between SFGs and passive galaxies, $\log(\mathrm{sSFR}) = -10.8\ \mathrm{yr}^{-1}$. The redshift value for the MS was adopted to be the median redshift of the SFGs in this sample of comparison galaxies, as discussed in M. B. Stone et al. (2023). For reference, the green valley transition region is marked per S. Salim (2014) with a green dashed box (for $z \sim 0$). Bottom: residuals that show the logarithmic difference (dex) between the quasar sSFR values and the sSFR values from the reference MS relation (orange dotted line), $\Delta(\mathrm{dex}) = \log_{10}(\mathrm{sSFR}_{\mathrm{quasar}}/\mathrm{sSFR}_{\mathrm{ref}})$. The plotted sSFR and stellar mass data for comparison galaxies come from the GAMA survey MAGPHYS SED analysis, while for quasar hosts from CIGALE SED fits. For quasar hosts, the sSFR values from CIGALE were corrected to the MAGHPYS baseline.

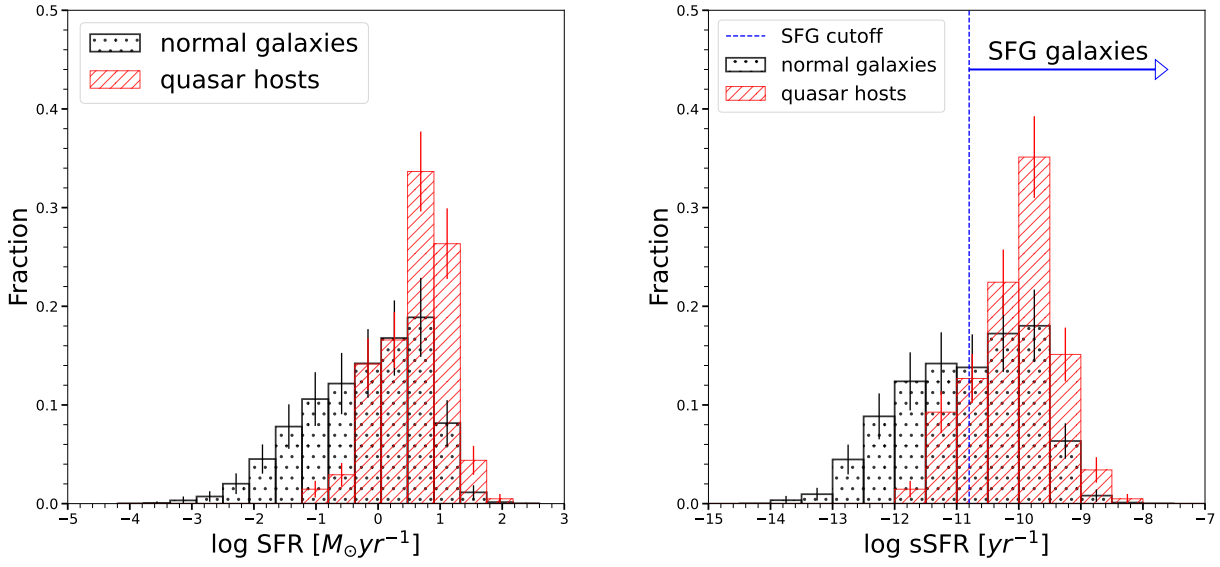

(a) (b)

Figure 10. Histograms of star formation properties with Poisson error bars: (a) SFR, (b) sSFR. Data for comparison galaxies are from the GAMA archive, for quasar hosts from CIGALE SED fits. For quasar hosts, CIGALE SFR and sSFR estimates are corrected to the MAGPHYS baseline, and the error bar represents the Poisson error. For comparison galaxies, the plotted fraction in each bin is the average fraction from all 200 realizations, and the error bar represents the standard deviation. In each case, the distribution of values for the quasar sample lies at the peak of the normal galaxy distribution. However, there are few quenched AGN hosts.

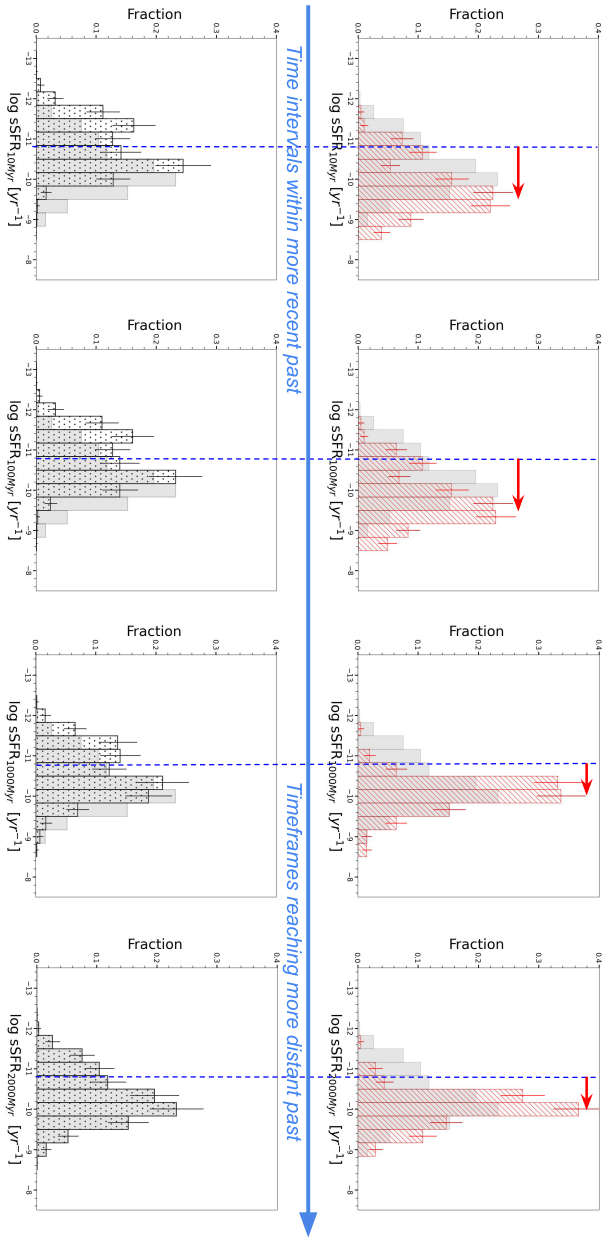

Figure 11. Histograms of sSFR averaged over 10, 100, 1000, and 2000 Myr for quasars (red hashed bars) and for normal galaxies (black dotted bars). For quasars, average sSFR estimates from CIGALE for 10 Myr and 100 Myr are corrected to MAGPHYS baseline. For visual contrast, the 2 Gyr distribution for normal galaxies is shown in shaded bars in each plot. Error bars as in Figure 10. The plots are arranged along the increasing timescale over which SFR is averaged. To highlight the comparison and the evolution of the distributions, the blue dashed line marks the sSFR $= -10.8$ yr^{-1} line in all plots, while the red arrow on quasar plots shows the separation from the approximate peak of the distribution. Thus, the quasar host sample exhibits elevated SFR values at 100 and 10 Myr marks. Note that the SFR peak for quasar hosts is moved toward higher values in more recent time frames. On the other hand, there is no evidence that the SFR of normal galaxies is changing with time. Indeed, it seems that the star-forming cloud is always in the same place, even at high redshift.

population. Of course, this might not be the case for very powerful quasars and radio galaxies that are rarer and will only rarely be present in volumes the size of the GAMA survey.

When we compare with the distribution for SFGs, we note that there is a smaller fraction of quasar host galaxies in the green valley, with a few quasars lying at the top end of the quiescent galaxies distribution. This suggests that star formation may be quenched in otherwise normal SFGs. An alternate hypothesis to explain the deficit of quasar host galaxies in the green valley would be that quasar host galaxies initially lie in the green valley and undergo increased SFR later. In order to test this, we can look at the averaged SFR over the past 10 and 100 Myr and then compare the star formation timescales to the expected quasar lifetimes, discussed next.

5.2. Quasar Hosts Show an Increase in Star Formation at Recent Timescales

It is interesting to consider the timescale for star formation and compare it with the expected quasar lifetimes. In the model of A. M. Hopkins & J. F. Beacom (2006) quasars are associated with increased star formation over a timescale of $\sim$10 Myr followed by quenching once the quasar becomes optically bright (see also K. A. Morey et al. 2021).

The SFR and sSFR distributions for non-AGN galaxies (CSNG) appear to be relatively similar at all times, suggesting that these objects have undergone a comparatively quiet evolution since $z \sim 0.3$, as demonstrated by the sequence of bottom panels in Figure 11. Similarly, this is the case for the SFR and sSFR distributions for quasar host galaxies for timescales of 1000 and 2000 Myr (top rightmost panels in Figure 11).

In contrast, there is evidence of an increase in SFRs in quasar host galaxies within the last 100 Myr and 10 Myr (top leftmost panels in Figure 11). We see that the SFR and sSFR distributions for quasar host galaxies are shifted toward higher values over more recent timescales, implying an association between an increase in star formation activity and nuclear activity. Note that if the SFR averaged over 1000 and 2000 Myr is overestimated for quasar hosts by MAGPHYS, then the resultant increase in star formation is even more profound, and thus does not reverse the conclusions of this work.

We stress that all quasar host galaxies, however, were forming stars on the star-forming main sequence (MS) within the last 2 Gyr. In other words, quasar activity is associated with an increase in SFRs in already normal SFGs. Increased SFR is therefore associated with quasar activity, but the starburst entity is modest, similar to the episodic SFR encountered in normal spirals.

5.3. Deficit of Quasar Host Galaxies in the Green Valley Region

Let us consider again the sSFR versus stellar mass diagram (Figure 9), which shows that there is a relative deficit of quasar host galaxies (compared to SFGs and all galaxies) in the traditional green valley region and the quiescent region. The distribution of SFRs for quasar host galaxies appears bimodal, with a small fraction of objects in the quiescent portion of the sSFR–stellar mass plot, but lying close to the sSFR limit for galaxies to be identified as star-forming. This hints that quasar host galaxies may have been more quiescent prior to the activation of the AGN and closer to the green valley, as argued by M. Pović et al. (2012). However, the older stellar populations of quasar host galaxies are not significantly different from those of normal galaxies (Figure 12). Nevertheless, quasar host galaxies have always been star-forming

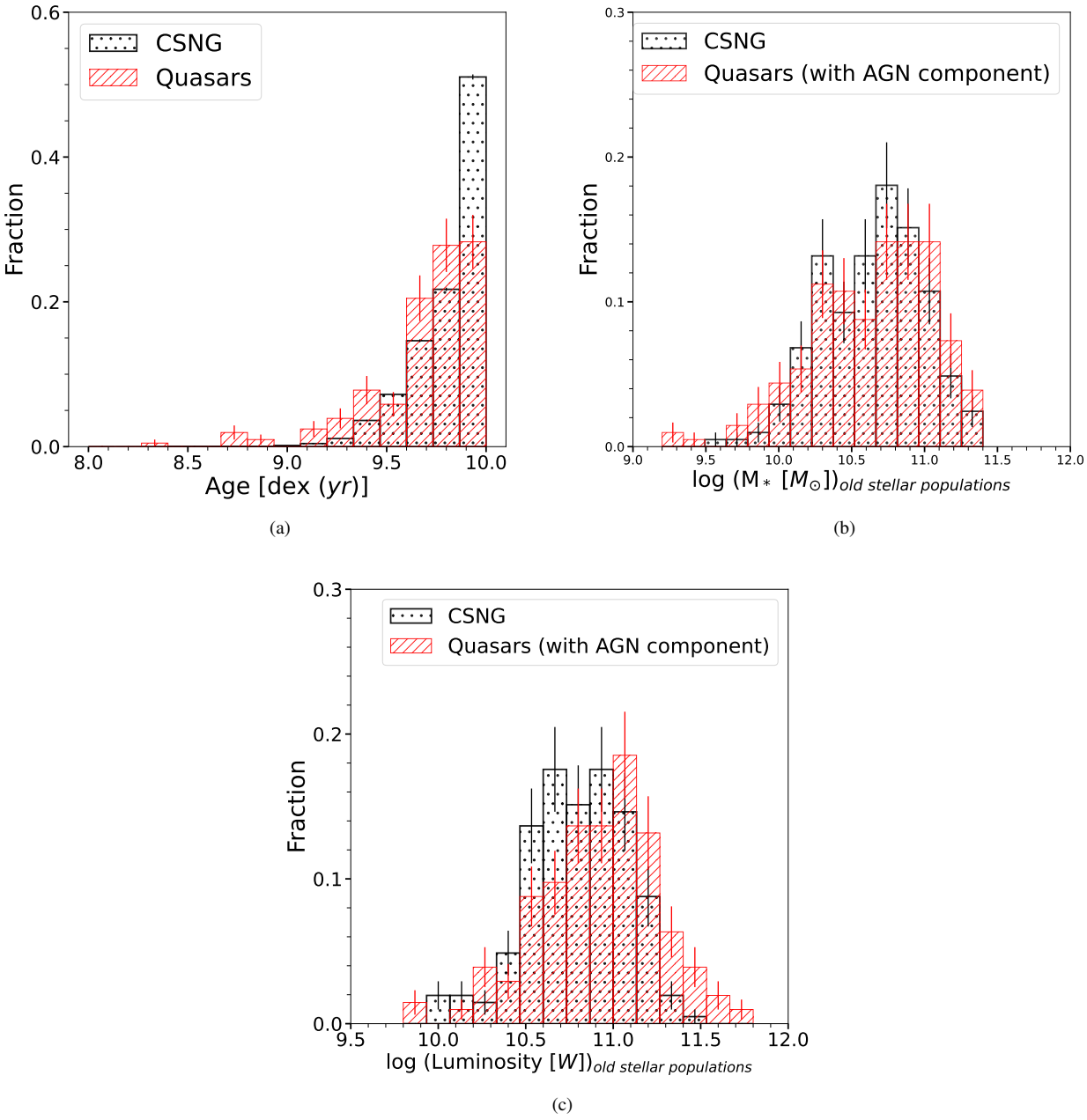

Figure 12. Histograms for old stellar populations for both the quasar sample (red hatched bars) and for the CSNG (black dotted bars). (a) Age of the oldest stars in the galaxy from MAGPHYS fits. (b) Stellar mass and (c) luminosity of old populations from CIGALE fits. The error bars are as in Figure 10.

over these timescales, lending support to models where nuclear activity is triggered by secular evolution.

5.4. Implications for Models Linking SFR and AGN Activity

Our finding that most quasar host galaxies lie on or close to the star-forming MS is consistent with the observations by I. Smirnova-Pinchukova et al. (2022), where no significant effect was found on the SFRs of quasar host galaxies. Coupled with the lack of quiescent galaxies among quasar hosts (although there may be radio galaxies that do not fulfill the criteria for inclusion by C. Gattano et al. 2018), this is consistent with recent studies suggesting that there is no significant effect from feedback by active nuclei (D. Elbaz et al. 2011; A. Bongiorno et al. 2012; C. M. Harrison et al. 2012; B. Balmaverde et al. 2016; T. K. D. Leung et al. 2017; J.-H. Woo et al. 2017; J. Shangguan et al. 2018; J. Scholtz et al. 2020). M.-Y. Zhuang & L. C. Ho (2022) also find vast majority of quasar host galaxies are star-forming, while L. Koutoulidis et al. (2022) claim that three-quarters of their X-ray-selected AGN lie on or above the star-forming MS, but J. Shangguan et al. (2020a, 2020b) and Y. Xie et al. (2021) argue that the SFRs of quasar host galaxies in their Palomar–Green sample approximate those of starbursts. G. Mountrichas et al. (2024a, 2024b) also find that only quasars with high X-ray luminosity have higher SFRs than comparable nonactive galaxies.

About one-quarter of quasar hosts are transitioning from star-forming to the quenched population of galaxies; they all have [O II] emission, but this is not securely associated with current star formation, as the spectra may be contaminated with emission from the nuclear region. This is an indication

that nuclear activity may continue for a considerable time after star formation is quenched (as in S. B. Rembold et al. 2017; S. F. Sánchez et al. 2018).

T. Goto (2006) claims that about 5% of quasars show post-starburst signatures. Post-starburst signatures are more recently observed also in the off-center optical spectra of low-z Type I quasar hosts (D. Bettoni et al. 2017; M. B. Stone et al. 2021). In this case, nuclear activity continues for a considerable time after quenching, since the presence of post-starburst features implies that star formation ceased a few hundred Myr ago. This is in contrast to the simple model, where quasars drive rapid quenching by feedback and then dwindle.

However, we can also show that most of the increase in SFRs has taken place over the past ∼100 Myr, while all quasar host galaxies are seen to be normal SFGs over the past 1–2 Gyr. None of the quasar hosts was originally quiescent. Therefore, this argues that the AGN activity is related to an increase in SFRs in otherwise normal galaxies. Deep integral field unit and long slit spectra of nearby AGNs show that peak AGN activity occurs ∼50–200 Myr after the onset of star formation (R. I. Davies et al. 2007; R. Riffel et al. 2022; see also K. Schawinski et al. 2009; V. Wild et al. 2010). Similar timescales are seen in S. B. Rembold et al. (2017) and S. F. Sánchez et al. (2018). This is consistent with our findings that star formation in quasar host galaxies has increased over the past 100 Myr.

The star-forming region may provide the fuel for the SMBH and allow such fuel to reach the SMBH via increased turbulence. Analytical models, numerical simulations, and hydrodynamical simulations predict that stellar winds and supernovae will enhance the SMBH mass accretion by injecting turbulence into the gas disk (e.g., K. Wada et al. 2002; M. Schartmann et al. 2009; A. Hobbs et al. 2011) while several authors have now reported a correlation between the black hole accretion rate and increasing SFRs (J. R. Mullaney et al. 2012; C.-T. J. Chen et al. 2013; K. Harris et al. 2016; G. Lanzuisi et al. 2017; M.-Y. Zhuang & L. C. Ho 2020; M.-Y. Zhuang et al. 2021). This association between quasars and star formation need not be causal: it may simply reflect the availability of a large gas supply, some of which is driven to the nucleus to fuel the AGN (M. E. Jarvis et al. 2020; J. Shangguan et al. 2020a; H. M. Yesuf & L. C. Ho 2020).

Based on what we see in Figures 10–12, we suggest that the recent increase in star formation and AGN activity may have occurred among galaxies in the green valley, where quasar host galaxies seem to be less frequent. These galaxies may experience an increase in star formation, and this may then induce quasar activity, as argued by M. Pović et al. (2012), P. J. L. Charlton et al. (2019), and X. Lin et al. (2022), where X-ray-selected AGN are observed preferentially in the green valley region (i.e., at lower SFRs). The SFR increase may be episodic, as is observed in many spiral galaxies, rather than due to mergers and interactions, although these could certainly play a role as in our Galaxy (T. Ruiz-Lara et al. 2020). Gas from young stars may then feed AGN activity, explaining the observations in Figures 10–12. This may also explain the different claims about the correlation between star formation, quenching, and quasar activity, if samples are chosen in different portions of this life cycle.

It is unclear what mechanisms may produce an increase in the SFR and fuel the AGN. Major mergers are clearly able to induce strong tidal torques and drive gas and dust to the center, but they are likely to be important only for the most powerful AGN. There is no strong evidence that quasar host galaxies are more morphologically disturbed than normal galaxies of the same luminosity (N. A. Grogin et al. 2005; B. McKernan et al. 2010; M. Cisternas et al. 2011; D. D. Kocevski et al. 2012; A. Böhm et al. 2013; C. Villforth et al. 2014, 2019; V. Marian et al. 2019; E. A. Shah et al. 2020). It has been shown that quasar host galaxies favor relatively low-density environments (C. F. Wethers et al. 2022) and do not have significantly more or fewer companions (M. B. Stone et al. 2023), while the star formation properties and stellar populations of galaxies neighboring quasar hosts are consistent with those of normal galaxies of the same mass (D. Bettoni et al. 2017, 2023; M. B. Stone et al. 2021, 2023).

This leaves minor mergers and secular evolution, such as bars and spiral arms (I. Shlosman et al. 1989; P. F. Hopkins & E. Quataert 2010) as possible triggers (this conclusion stands even though GAMA has few massive cluster environments). These suffice to fuel most of AGN activity (e.g., L. C. Ho 2009; M. Cisternas et al. 2011; C. Villforth et al. 2017; Y. Zhao et al. 2022). The timescales we find here are long enough to favor such gentler and slower processes.

6. Conclusions

In this work, we investigated the SFH of low-redshift ($0.1 < z < 0.35$) Type I AGN within the GAMA volume and compared these objects to nonactive galaxies in the same survey matched in redshift and stellar mass. Our main conclusions are as follows.

1. Most (80%) quasars lie on the star-forming MS for normal galaxies, and 20% are hosted in quenching or quenched systems.
2. The SFHs of these quasar host galaxies show that they have generally been SFGs over the past 2 Gyr but have experienced a modest star formation increase (by a factor of 2–3) over the past 100 Myr.
3. These observations support models where star formation feeds quasar activity, and its cessation starves the SMBH of gas and dust, leading to its undergoing a quiescent state.
4. We conclude that the correlation between the SMBH mass and the bulge mass may not have a causal relation and that AGN activity, at least in the local universe, is mainly triggered by secular processes within normal galaxies.

Extending this analysis to a much larger quasar sample is necessary to more definitively validate the conclusions of this work. For example, future work is planned with the quasars surveyed by the Dark Energy Spectroscopic Instrument (DESI Collaboration et al. 2016).

Acknowledgments

M.B.S. acknowledges the Finnish Cultural Foundation grant Nos. 00220968 and 00231098, the Academy of Finland grant No. 311438, and FINCA funding. M.B.S. acknowledges useful email discussions with Pekka Heinämäki, Johanna Hartke, Véronique Buat, Denis Burgarella, Kostas Kouroumpatzakis, Elina Lindfors, Talvikki Hovatta, and with GAZPAR support personnel for CIGALE, operated by CeSAM-LAM and IAP,

support for GAMA survey questions from Ivan Baldry, Simon Driver, Jonathan Loveday, and Alister Graham, and James Stone, Kaj Wiik for help with the CIGALE installation, science discussions with the FINCA community, and feedback from the referee.

GAMA is a joint European-Australasian project based around a spectroscopic campaign using the Anglo-Australian Telescope. The GAMA input catalog is based on data taken from SDSS and the UKIRT Infrared Deep Sky Survey. Complementary imaging of the GAMA regions is being obtained by a number of independent survey programs, including the Galaxy Evolution Explorer (GALEX) Medium Imaging Survey (MIS), VLT Survey Telescope, KiDS, Visible and Infrared Survey Telescope for Astronomy (VISTA) Kilo-Degree Infrared Galaxy Survey (VIKING), Wide-Field Infrared Survey Explorer (WISE), Herschel-ATLAS, GMRT, and ASKAP, providing UV to radio coverage. GAMA is funded by the STFC (UK), the ARC (Australia), the AAO, and the participating institutions. The GAMA website is at http://www.gama-survey.org/.

This research has made use of the Spanish Virtual Observatory (https://svo.cab.inta-csic.es) project funded by MCIN/AEI/10.13039/501100011033/ through grant PID2020-112949GB-I00; the NASA/IPAC Extragalactic Database (NED), which is funded by the National Aeronautics and Space Administration and operated by the California Institute of Technology; StackOverflow platform, the VizieR database (F. Ochsenbein et al. 2000); Cosmology Calculator (E. L. Wright 2006), Seafile file collaboration platform.

Faciliity: AAT (Anglo-Australian Telescope).

Software: ASTROPY (Astropy Collaboration et al. 2013, 2018), MATPLOTLIB (J. D. Hunter 2007), NUMPY (C. R. Harris et al. 2020), PYTHON (G. Van Rossum & F. L. Drake 2009), SEABORN (M. L. Waskom 2021), SCIPY (P. Virtanen et al. 2020), and code from M. B. Stone (2017). The associated code is released with open access as a minimal code example (M. B. Stone 2025a) and as the detailed calculations (M. B. Stone 2025b), with ASCL identifiers correspondingly ASCL:2511.002; ASCL:2511.003.

ORCID iDs

Maria B. Stone https://orcid.org/0000-0002-2931-0593
Roberto De Propris https://orcid.org/0000-0003-1455-7339
Clare Wethers https://orcid.org/0000-0002-7135-2842
Jari Kotilainen https://orcid.org/0000-0003-0133-7644
Nischal Acharya https://orcid.org/0000-0001-9738-3594
Benne Holwerda https://orcid.org/0000-0002-4884-6756
Andrew M. Hopkins https://orcid.org/0000-0002-6097-2747
Kevin Pimbblet https://orcid.org/0000-0002-3963-3919

References

Abazajian, K. N., Adelman-McCarthy, J. K., Agüeros, M. A., et al. 2009, ApJS, 182, 543
Asari, N. V., Cid Fernandes, R., Stasińska, G., et al. 2007, MNRAS, 381, 263
Astropy Collaboration, Price-Whelan, A. M., Sipőcz, B. M., et al. 2018, AJ, 156, 123
Astropy Collaboration, Robitaille, T. P., Tollerud, E. J., et al. 2013, A&A, 558, A33
Balmaverde, B., Marconi, A., Brusa, M., et al. 2016, A&A, 585, A148
Barger, A. J., Cowie, L. L., Owen, F. N., et al. 2015, ApJ, 801, 87
Bettoni, D., Falomo, R., Kotilainen, J. K., & Karhunen, K. 2017, MNRAS, 466, 3600
Bettoni, D., Falomo, R., Kotilainen, J. K., Karhunen, K., & Uslenghi, M. 2015, MNRAS, 454, 4103
Bettoni, D., Falomo, R., Paiano, S., Kotilainen, J. K., & Stone, M. B. 2023, MNRAS, 519, 2929
Bieri, R., Dubois, Y., Silk, J., Mamon, G. A., & Gaibler, V. 2016, MNRAS, 455, 4166
Blandford, R., Meier, D., & Readhead, A. 2019, ARA&A, 57, 467
Böhm, A., Wisotzki, L., Bell, E. F., et al. 2013, A&A, 549, A46
Bongiorno, A., Merloni, A., Brusa, M., et al. 2012, MNRAS, 427, 3103
Boquien, M., Burgarella, D., Roehlly, Y., et al. 2019, A&A, 622, A103
Bruzual, G., & Charlot, S. 2003, MNRAS, 344, 1000
Burgarella, D., Buat, V., & Iglesias-Páramo, J. 2005, MNRAS, 360, 1413
Calzetti, D., Armus, L., Bohlin, R. C., et al. 2000, ApJ, 533, 682
Chabrier, G. 2003, ApJL, 586, L133
Charlot, S., & Fall, S. M. 2000, ApJ, 539, 718
Charlton, P. J. L., Ruan, J. J., Haggard, D., et al. 2019, ApJ, 876, 75
Chen, C.-T. J., Hickox, R. C., Alberts, S., et al. 2013, ApJ, 773, 3
Ciesla, L., Charmandaris, V., Georgakakis, A., et al. 2015, A&A, 576, A10
Circosta, C., Mainieri, V., Padovani, P., et al. 2018, A&A, 620, A82
Cisternas, M., Jahnke, K., Inskip, K. J., et al. 2011, ApJ, 726, 57
Conroy, C. 2013, ARA&A, 51, 393
Cresci, G., Mainieri, V., Brusa, M., et al. 2015, ApJ, 799, 82
da Cunha, E., & Charlot, S., 2011 MAGPHYS: Multi-wavelength Analysis of Galaxy Physical Properties, Astrophysics Source Code Library, ascl:1106.010
da Cunha, E., Charlot, S., & Elbaz, D. 2008, MNRAS, 388, 1595
Dale, D. A., Helou, G., Magdis, G. E., et al. 2014, ApJ, 784, 83
Davies, R. I., Müller Sánchez, F., Genzel, R., et al. 2007, ApJ, 671, 1388
DESI Collaboration, Aghamousa, A., Aguilar, J., et al. 2016, arXiv:1611.00036
Driver, S. P., Andrews, S. K., da Cunha, E., et al. 2018, MNRAS, 475, 2891
Driver, S. P., Bellstedt, S., Robotham, A. S. G., et al. 2022, MNRAS, 513, 439
Driver, S. P., Wright, A. H., Andrews, S. K., et al. 2016, MNRAS, 455, 3911
Eales, S., Dunne, L., Clements, D., et al. 2010, PASP, 122, 499
Edge, A., Sutherland, W., Kuijken, K., et al. 2013, Msngr, 154, 32
El-Badry, K., Wetzel, A., Geha, M., et al. 2016, ApJ, 820, 131
Elbaz, D., Dickinson, M., Hwang, H. S., et al. 2011, A&A, 533, A119
Fabian, A. C. 2012, ARA&A, 50, 455
Falomo, R., Bettoni, D., Karhunen, K., Kotilainen, J. K., & Uslenghi, M. 2014, MNRAS, 440, 476
Gattano, C., Andrei, A. H., Coelho, B., et al. 2018, A&A, 614, A140
Gebhardt, K., Bender, R., Bower, G., et al. 2000, ApJL, 539, L13
Georgantopoulos, I., Pouliasis, E., Mountrichas, G., et al. 2023, A&A, 673, A67
Gofford, J., Reeves, J. N., McLaughlin, D. E., et al. 2015, MNRAS, 451, 4169
Goto, T. 2006, MNRAS, 369, 1765
Graham, A. W., Jarrett, T. H., & Cluver, M. E. 2024, MNRAS, 527, 10059
Granato, G. L., De Zotti, G., Silva, L., Bressan, A., & Danese, L. 2004, ApJ, 600, 580
Grogin, N. A., Conselice, C. J., Chatzichristou, E., et al. 2005, ApJL, 627, L97
Gültekin, K., Richstone, D. O., Gebhardt, K., et al. 2009, ApJ, 698, 198
Harris, C. R., Millman, K. J., van der Walt, S. J., et al. 2020, Natur, 585, 357
Harris, K., Farrah, D., Schulz, B., et al. 2016, MNRAS, 457, 4179
Harrison, C. M., Alexander, D. M., Mullaney, J. R., et al. 2012, ApJL, 760, L15
Ho, L. C. 2009, ApJ, 699, 626
Hobbs, A., Nayakshin, S., Power, C., & King, A. 2011, MNRAS, 413, 2633
Hopkins, A. M., & Beacom, J. F. 2006, ApJ, 651, 142
Hopkins, P. F. 2012, MNRAS, 420, L8
Hopkins, P. F., & Quataert, E. 2010, MNRAS, 407, 1529
Hopkins, P. F., Torrey, P., Faucher-Giguère, C.-A., Quataert, E., & Murray, N. 2016, MNRAS, 458, 816
Hunt, L. K., De Looze, I., Boquien, M., et al. 2019, A&A, 621, A51
Hunter, J. D. 2007, CSE, 9, 90
Husemann, B., Jahnke, K., Sánchez, S. F., et al. 2014, MNRAS, 443, 755
Ilbert, O., Arnouts, S., Le Floc'h, E., et al. 2015, A&A, 579, A2
Ishibashi, W., & Fabian, A. C. 2012, MNRAS, 427, 2998
Jahnke, K., & Macciò, A. V. 2011, ApJ, 734, 92
Jarvis, M. E., Harrison, C. M., Mainieri, V., et al. 2020, MNRAS, 498, 1560
Jin, J.-J., Zhu, Y.-N., Meng, X.-M., Lei, F.-J., & Wu, H. 2018, ApJ, 864, 32
Karhunen, K., Kotilainen, J. K., Falomo, R., & Bettoni, D. 2014, MNRAS, 441, 1802
Katsianis, A., Zheng, X., Gonzalez, V., et al. 2019, ApJ, 879, 11
Kauffmann, G., Heckman, T. M., White, S. D. M., et al. 2003, MNRAS, 341, 54
Kawakatu, N., & Wada, K. 2008, ApJ, 681, 73
King, A., & Pounds, K. 2015, ARA&A, 53, 115
Kocevski, D. D., Faber, S. M., Mozena, M., et al. 2012, ApJ, 744, 148

Kormendy, J., & Ho, L. C. 2013, ARA&A, 51, 511
Koutoulidis, L., Mountrichas, G., Georgantopoulos, I., Pouliasis, E., & Plionis, M. 2022, A&A, 658, A35
Lanzuisi, G., Delvecchio, I., Berta, S., et al. 2017, A&A, 602, A123
Leung, T. K. D., Riechers, D. A., & Pavesi, R. 2017, ApJ, 836, 180
Lin, X., Xue, Y., Fang, G., et al. 2022, RAA, 22, 015010
Liske, J., Baldry, I. K., Driver, S. P., et al. 2015, MNRAS, 452, 2087
Lutz, D., Mainieri, V., Rafferty, D., et al. 2010, ApJ, 712, 1287
Magorrian, J., Tremaine, S., Richstone, D., et al. 1998, AJ, 115, 2285
Mandal, A., Mukherjee, D., Federrath, C., et al. 2021, MNRAS, 508, 4738
Marian, V., Jahnke, K., Mechtley, M., et al. 2019, ApJ, 882, 141
Martin, D. C., Fanson, J., Schiminovich, D., et al. 2005, ApJL, 619, L1
McKernan, B., Ford, K. E. S., & Reynolds, C. S. 2010, MNRAS, 407, 2399
McLure, R. J., Kukula, M. J., Dunlop, J. S., et al. 1999, MNRAS, 308, 377
Morey, K. A., Eilers, A.-C., Davies, F. B., Hennawi, J. F., & Simcoe, R. A. 2021, ApJ, 921, 88
Mountrichas, G., Masoura, V. A., Corral, A., & Carrera, F. J. 2024a, A&A, 683, A143
Mountrichas, G., Masoura, V. A., Xilouris, E. M., et al. 2022a, A&A, 661, A108
Mountrichas, G., Buat, V., Yang, G., et al. 2022b, A&A, 667, A145
Mountrichas, G., Siudek, M., & Cucciati, O. 2024b, A&A, 686, A229
Mullaney, J. R., Daddi, E., Béthermin, M., et al. 2012, ApJL, 753, L30
Nayakshin, S., & Zubovas, K. 2012, MNRAS, 427, 372
Nolan, L. A., Dunlop, J. S., Kukula, M. J., et al. 2001, MNRAS, 323, 308
Noll, S., Burgarella, D., Giovannoli, E., et al. 2009, A&A, 507, 1793
Ochsenbein, F., Bauer, P., & Marcout, J. 2000, A&AS, 143, 23
Page, M. J., Symeonidis, M., Vieira, J. D., et al. 2012, Natur, 485, 213
Pâris, I., Petitjean, P., Aubourg, É., et al. 2018, A&A, 613, A51
Paspaliaris, E. D., Xilouris, E. M., Nersesian, A., et al. 2023, A&A, 669, A11
Planck Collaboration, Aghanim, N., Akrami, Y., et al. 2020, A&A, 641, A6
Pović, M., Sánchez-Portal, M., Pérez García, A. M., et al. 2012, A&A, 541, A118
Rakshit, S., Stalin, C. S., Chand, H., & Zhang, X.-G. 2017, ApJS, 229, 39
Rembold, S. B., Shimoia, J. S., Storchi-Bergmann, T., et al. 2017, MNRAS, 472, 4382
Riffel, R., Dahmer-Hahn, L. G., Riffel, R. A., et al. 2022, MNRAS, 512, 3906
Riffel, R. A., Storchi-Bergmann, T., Dors, O. L., & Winge, C. 2009, MNRAS, 393, 783
Rosario, D. J., Santini, P., Lutz, D., et al. 2012, A&A, 545, A45
Ruiz-Lara, T., Gallart, C., Bernard, E. J., & Cassisi, S. 2020, in XIV.0 Scientific Meeting (Virtual) of the Spanish Astronomical Society, 185, (Spanish Astronomical Society) https://www.sea-astronomia.es/reunion-cientifica-2020
Salim, S. 2014, SerAJ, 189, 1
Sánchez, S. F., Avila-Reese, V., Hernandez-Toledo, H., et al. 2018, RMxAA, 54, 217
Santini, P., Rosario, D. J., Shao, L., et al. 2012, A&A, 540, A109
Sarzi, M., Allard, E. L., Knapen, J. H., & Mazzuca, L. M. 2007, MNRAS, 380, 949
Schartmann, M., Meisenheimer, K., Klahr, H., et al. 2009, MNRAS, 393, 759
Schawinski, K., Virani, S., Simmons, B., et al. 2009, ApJL, 692, L19
Scholtz, J., Harrison, C. M., Rosario, D. J., et al. 2020, MNRAS, 492, 3194
Shah, E. A., Kartaltepe, J. S., Magagnoli, C. T., et al. 2020, ApJ, 904, 107
Shangguan, J., Ho, L. C., Bauer, F. E., Wang, R., & Treister, E. 2020a, ApJ, 899, 112
Shangguan, J., Ho, L. C., Bauer, F. E., Wang, R., & Treister, E. 2020b, ApJS, 247, 15
Shangguan, J., Ho, L. C., & Xie, Y. 2018, ApJ, 854, 158
Shimizu, T. T., Mushotzky, R. F., Meléndez, M., Koss, M., & Rosario, D. J. 2015, MNRAS, 452, 1841
Shin, J., Woo, J.-H., Chung, A., et al. 2019, ApJ, 881, 147
Shlosman, I., Frank, J., & Begelman, M. C. 1989, Natur, 338, 45
Silk, J., & Rees, M. J. 1998, A&A, 331, L1
Smirnova-Pinchukova, I., Husemann, B., Davis, T. A., et al. 2022, A&A, 659, A125
Stalevski, M., Fritz, J., Baes, M., Nakos, T., & Popović, L. 2012, MNRAS, 420, 2756
Stalevski, M., Ricci, C., Ueda, Y., et al. 2016, MNRAS, 458, 2288
Stanley, F., Alexander, D. M., Harrison, C. M., et al. 2017, MNRAS, 472, 2221
Stanley, F., Harrison, C. M., Alexander, D. M., et al. 2015, MNRAS, 453, 591
Stemo, A., Comerford, J. M., Barrows, R. S., et al. 2020, ApJ, 888, 78
Stone, M. B. 2017, Master's thesis, San Jose State Univ. doi:10.31979/etd.y5dm-j3p4
Stone, M. B., 2025a sndik16/SFR_ChebyFit_example: v1.0, Zenodo, doi:10.5281/zenodo.17381578
Stone, M. B., 2025b sndik16/GAMA_quasarhosts_starformation: v1.0, Zenodo, doi:10.5281/zenodo.17405203
Stone, M. B., 2025c SFR_ChebyFit_example: Chebyshev-based correction of SFR estimators, Astrophysics Source Code Library, ascl:2511.002
Stone, M. B., 2025d GAMA Quasar Hosts: Star formation analysis pipeline, Astrophysics Source Code Library, ascl:2511.003
Stone, M. B., Bettoni, D., Falomo, R., et al. 2021, MNRAS, 501, 419
Stone, M. B., Wethers, C. F., de Propris, R., et al. 2023, ApJ, 946, 116
Suh, H., Civano, F., Hasinger, G., et al. 2017, ApJ, 841, 102
Terrazas, B. A., Bell, E. F., Pillepich, A., et al. 2020, MNRAS, 493, 1888
Trussler, J., Maiolino, R., Maraston, C., et al. 2020, MNRAS, 491, 5406
Van Rossum, G., & Drake, F. L. 2009, Python 3 Reference Manual (CreateSpace)
Véron-Cetty, M. P., & Véron, P. 2010, A&A, 518, A10
Villforth, C., Hamann, F., Rosario, D. J., et al. 2014, MNRAS, 439, 3342
Villforth, C., Hamilton, T., Pawlik, M. M., et al. 2017, MNRAS, 466, 812
Villforth, C., Herbst, H., Hamann, F., et al. 2019, MNRAS, 483, 2441
Virtanen, P., Gommers, R., Oliphant, T. E., et al. 2020, NatMe, 17, 261
Wada, K., Meurer, G., & Norman, C. A. 2002, ApJ, 577, 197
Wang, X., & Loeb, A. 2018, NewA, 61, 95
Waskom, M. L. 2021, JOSS, 6, 3021
Wethers, C. F., Acharya, N., De Propris, R., et al. 2022, ApJ, 928, 192
Wild, V., Heckman, T., & Charlot, S. 2010, MNRAS, 405, 933
Woo, J.-H., Son, D., & Bae, H.-J. 2017, ApJ, 839, 120
Wright, A. H., Robotham, A. S. G., Bourne, N., et al. 2016, MNRAS, 460, 765
Wright, E. L. 2006, PASP, 118, 1711
Wright, E. L., Eisenhardt, P. R. M., Mainzer, A. K., et al. 2010, AJ, 140, 1868
Xie, Y., Ho, L. C., Zhuang, M.-Y., & Shangguan, J. 2021, ApJ, 910, 124
Yang, C., Ge, J.-Q., & Lu, Y.-J. 2019, RAA, 19, 177
Yang, G., Boquien, M., Brandt, W. N., et al. 2022, ApJ, 927, 192
Yesuf, H. M., & Ho, L. C. 2020, ApJ, 901, 42
Zhao, Y., Li, Y. A., Shangguan, J., Zhuang, M.-Y., & Ho, L. C. 2022, ApJ, 925, 70
Zhuang, M.-Y., & Ho, L. C. 2020, ApJ, 896, 108
Zhuang, M.-Y., & Ho, L. C. 2022, ApJ, 934, 130
Zhuang, M.-Y., Ho, L. C., & Shangguan, J. 2021, ApJ, 906, 38
Zubovas, K., & Bourne, M. A. 2017, MNRAS, 468, 4956
Zubovas, K., Nayakshin, S., King, A., & Wilkinson, M. 2013, MNRAS, 433, 3079